PERGAMON

International Journal of Heat and Mass Transfer 45 (2002) 5069–5081

International Journal of HEAT and MASS TRANSFER

www.elsevier.com/locate/ijhmt

Spectrally correlated radiation and laminar forced convection in the entrance region of a circular duct

EzEddine Sediki [a], Anouar Soufiani [b,*], Mohamed Salah Sifaoui [a]

[a] *Laboratoire de Rayonnement Thermique, Faculté des Sciences de Tunis, 1060 Tunis, Tunisie*

[b] *Laboratoire d'Énergétique Moléculaire et Macroscopique, Combustion (EM2C), UPR 288 du CNRS, École Centrale Paris, 92295 Châtenay-Malabry Cedex, France*

Received 24 November 2000; received in revised form 27 March 2002

Abstract

The two-dimensional combined radiative and convective transfer in emitting and absorbing real gases in the entrance region of a duct with a jump of wall temperature is studied. The axial propagation of radiation is taken into account in the analysis. The flow field and the energy equations are solved simultaneously and the radiative properties of the flowing gases, CO_2 or H_2O, are modeled by using either the narrow-band correlated-k model or the global absorption distribution function (ADF) model. The results are presented in terms of temperature and radiative power fields, and of the evolution of bulk temperatures and of heat transfer coefficients. Due to the axial component of the radiative flux, the gas is preheated or precooled before the change in wall temperature and this induces a persistent difference between the results of 1-D and 2-D radiation analyses. Some differences between CO_2 and H_2O temperature and radiative power profiles, due to the different structures of their spectra, are put in evidence. The ADF model, only suitable for gray walls, is shown to be less accurate when the gas is heated than when it is cooled.

1. Introduction

Examples of combined radiation, convection and/or conduction in absorbing and emitting media are found in applications such as industrial furnaces, combustion chambers, high-temperature heat exchangers, reentry applications, etc. The non-gray behavior of gases, the multidimensional nature of radiative transfer and the resulting coupling between different volume elements in the medium are the main fundamental difficulties introduced in the problem of combined heat transfer for real gases. The interaction of thermal radiation and forced convection in the thermal entrance region of circular and non-circular ducts with sudden temperature jump has been studied by many investigators [1–21] with various degrees of approximations. Other references in the general field may be found in classical textbooks or review papers (e.g., Refs. [22,23]).

We focus here our attention on studies considering multidimensional radiative transfer and/or realistic medium radiative properties. Only few researchers [1–7] have considered a radiation field accounting for the axial temperature variations in the entrance region, which induces an axial component of the radiative flux. Under the assumptions of fully developed laminar velocity distribution and constant thermophysical properties, Desoto [1] considered the interaction of two-dimensional radiation with conduction and convection in a non-isothermal, non-gray gas (CO_2) flowing in the entrance region of a tube with isothermal black walls by solving the integro-differential energy equation numerically. He concluded that although the axial radiative flux component is large at the tube entrance, it decreases rather abruptly as the flow proceeds only a short distance into the tube and its effect thereafter on temperature distributions is negligible. Using the finite difference technique, Echigo et al. [2] examined the combined transfer with a 2-D radiative analysis in a gray gas

* Corresponding author. Tel.: +33-141-131-071; fax: +33-147-028-035.

E-mail address: soufiani@em2c.ecp.fr (A. Soufiani).

0017-9310/02/$ - see front matter
PII: S0017-9310(02)00205-3

Nomenclature

a_j	weights in the ADF model
C_p	specific heat at constant pressure ($J\,kg^{-1}\,K^{-1}$)
D	diameter of the duct (m)
g_j	quadrature points in the CK model
H	heat transfer coefficient ($W\,m^{-2}\,K^{-1}$)
h	enthalpy per unit mass ($J\,kg^{-1}$)
I	radiative intensity ($W\,m^{-2}\,st^{-1}$)
k	reordered absorption coefficient (cm^{-1})
k^*	reduced absorption coefficient ($cm^{-1}\,atm^{-1}$)
l	discrete homogeneous and isothermal column length (cm)
l_0	upstream region length (m)
L	downstream region length (m)
p	pressure (Pa)
Pr	Prandtl number $= \mu C_p/\lambda$
Pe	Peclet number $= Re\,Pr$
q_r	radiative flux ($W\,m^{-2}$)
R	radius of the duct (m)
Re	Reynolds number $= u_0 D\rho/\mu$
s	curvilinear abscissa (m)
T	temperature (K)
T_b	bulk temperature (K)
u	axial velocity ($m\,s^{-1}$)
v	transverse velocity ($m\,s^{-1}$)
x	flow direction (m)
X	molar fraction of the absorbing species

Greek symbols

$\Delta\nu$	low-resolution spectral range (cm^{-1})
ϵ	emissivity
θ	directional discretization angle
κ	absorption coefficient ($cm^{-1}\,atm^{-1}$)
λ	molecular thermal conductivity ($W\,m^{-1}\,K^{-1}$)
μ	viscosity ($kg\,m^{-1}\,s^{-1}$)
ν	wave number (cm^{-1})
ρ	density ($kg\,m^{-3}$)
φ	heat flux per unit area ($W\,m^{-2}$)
ϕ	directional discretization angle
σ	Stefan Boltzmann constant ($W\,m^{-2}\,K^{-4}$)
ω_j	quadrature weights
Ω	solid angle

Subscripts

i	discretization over x-direction
j	discretization over absorption coefficient
ν	spectral quantity
g_j	quadrature point
ref	reference
o	inlet conditions
b	bands
ν_b	related to band $\Delta\nu_b$
r	radiative
tt	total
cd	conductive
w	wall

Superscripts

$-\Delta\nu$	mean properties over the spectral range $\Delta\nu$
°	equilibrium radiation

allowing an upstream propagation from the entrance of the hot tube wall. They compared the results of a two-dimensional radiative flux to those of a one-dimensional flux. They concluded that the local Nusselt numbers and the mixed mean temperatures obtained by the 1-D analysis are lower than those obtained by 2-D one near the entrance of the heating section in the region downstream the wall temperature jump. Kassemi and Chung [3] studied the two-dimensional combined convection and radiation transfer from a gray isotropically scattering fluid in a reflecting channel. They solved numerically the simultaneous non-linear integro-differential equations for a hydrodynamically fully developed flow using an element-to-node approach. Kim and Lee [4] analyzed the two-dimensional radiation in a thermally developing Poiseuille flow of a gray and anisotropically scattering fluid between infinite plane parallel plates. The radiative transfer equation (RTE) was solved by using the S–N discrete ordinates method. It was found that the two-dimensional effects are more pronounced when the channel optical thickness increases and when the conduction-radiation parameter and the scattering albedo decrease. A similar problem was analyzed by Huang and Lin [5]. The divergence of the radiative flux in a gray emitting and absorbing fluid was obtained by solving the two-dimensional radiation transfer by using the finite element node approximation technique. Yang and Edabian [6] treated the 2-D thermal radiation combined with forced convection in the entrance region in ducts for established laminar flow of a gray gas. The moment's method was applied to solve the radiation transfer equation. The authors proposed a criterion that serves to define the threshold of axial radiation effects at low-Peclet number.

The radiative properties of a molecular gas vary generally so strongly and rapidly across the spectrum and the gray gas approximation is today believed to be incorrect [22]. Many approximate radiative property models have been developed to represent molecular spectra of gases. The most accurate gas radiative prop-

erty model is the line-by-line (LBL) method, but this approach is generally not practicable in 2-D or 3-D geometries and in particular when radiative transfer is combined with other transfer modes since it requires large computational times and storage volumes. To circumvent this drawback, several narrow-band (statistical narrow band (SNB) [24], Correlated-k (CK) [25], Correlated-k with fictitious gases (CKFG) [26,27]), wide-band (exponential wide-band (EWB) model due to Edwards [28]) and global (spectral line-based weighted-sum-of-gray-gases (SLW) [29], absorption distribution function (ADF) [30]) gas infrared radiative property models have been introduced.

Recently, Pierrot et al. [31] and Pierrot [32] have studied the accuracy of narrow-band and global models applied to radiative transfer in a plane layer geometry with prescribed temperature profiles. It was shown that global models are generally slightly less accurate than band models, but are much more efficient in terms of CPU times. Concerning the studies related to combined radiation and convection cited above, the flowing gases were generally assumed to be gray [2–7,15–18] even if sometimes [15–18], the wave number independent absorption coefficient was deduced from parameters of the weighted sum of gray gases (WSGG) first introduced by Hottel (see Ref. [33]). Other authors have considered the box model [8,9,12,20] or a frequency-dependent absorption coefficient, issued from the EWB model but without taking into account the fine structure of gas absorption spectra [1,13,21]. To our knowledge, the only attempts to treat radiative transfer in a spectrally correlated manner are those of Edwards and co-workers [10,11], of Kim and Viskanta [14] and of Soufiani and Taine [19]. The EWB model was used in Refs. [10,11,14] while a SNB model was considered in Ref. [19] in association with the Curtis–Godson approximation for combined transfer in a laminar flow between two parallel isothermal plates. Unfortunately, the radiation axial component was neglected in these last studies.

To our knowledge, the effects of the axial radiative component in combined forced convection and radiation problems has never been analyzed for real gases. This is the main aim of the present study. We consider the flow of gaseous H_2O or CO_2 in a circular duct with a sudden jump of wall temperature. Preheating or precooling the gas before this temperature jump is allowed through the axial component of the radiative flux. Comparisons with 1-D radiation will be discussed.

In this paper special attention is devoted to the treatment of the spectral nature of radiation in real gases (H_2O or CO_2) at high temperature. The spectral correlation phenomenon is taken into account through the CK band model and the ADF global model. The results of these models are compared in the case of coupled radiative and convective strongly non-isothermal heating or cooling laminar gas flows. The choice of CK and ADF as narrow and global models results from their formulation in terms of absorption coefficients and then to their easier implementation in the computation of coupled problems.

The flow equations and energy balance equation are solved simultaneously with temperature-dependent fluid properties. To solve the mass, momentum and energy equations, an implicit finite difference technique is used. A discrete-direction method [34–36] is applied to solve the geometrical part of the radiative transfer problem.

Section 2 is devoted to the parameters of CK and ADF models and the way to use them in radiative transfer calculations. In Section 3, we present the basic equations of the problem and the numerical methods used to solve them. Comparisons between the results from 1-D and 2-D radiation analyses are given in Section 4 where we present temperature and radiative power profiles as well as heat transfer coefficients and the evolution of bulk temperatures. The comparisons between CK and ADF results are discussed in the same section.

2. Formulation and parameters of the CK and ADF models

The high-resolution structure of emission and absorption spectra of gases generates spectral correlation effects between emission, transmission and absorption by consecutive elementary columns. These effects strongly modify the local intensity field and consequently the radiative fluxes and the radiative power dissipated at each point of the medium. Approximate radiative property models can be classified into two main types: band models (SNB, CK, CKFG, EWB) and global models (WSGG, ADF, SLW). In band models, the spectrum is subdivided into spectral bands and average radiative properties are determined for each band. In global models, the entire spectrum is considered as a whole, but the walls and the particles, if present, must be assumed to be gray. The use of this last method leads to small computational times, but it has been considered to be generally slightly less accurate than band models [31].

In the present study, CK and ADF models are implemented for radiative transfer combined with laminar forced convection using the same method of solution of the RTE. The predictions of 1-D and 2-D radiative transfer from ADF is compared with CK predictions considered as a convenient and practicable reference in combined heat transfer problems. In fact, the accuracy of each model depends on its implementation. However, for similar numbers of absorption coefficient values in ADF and of quadrature points in CK, using the same spectroscopic data bases, and the same solver of the RTE, CK is more accurate than ADF since both models are founded on very similar correlation approximations

and CK is a narrow-band model while ADF is a global model. Thus, low-resolution spectral correlation effects are taken into account in CK approach and not necessarily in ADF. The same conclusion was drawn from the numerical tests of Pierrot et al. [31].

Parameters of CK and ADF models are deduced from LBL calculations founded on the same high-temperature EM2C spectroscopic data bases [37,38]. In the following, we provide some details related to CK and ADF parameters and to the practical way to use them in radiative transfer calculations. Details on model principles can be found in the references given below.

The CK model has been developed originally for atmospheric applications and is described in detail in Ref. [25]. Here, the radiative intensity $\bar{I}_v^{\Delta v}$ averaged over a spectral band of width Δv, is approximated by the seven points Gauss-type quadrature given in Ref. [39], i.e.:

$$\bar{I}_v^{\Delta v}(s) = \sum_{j=1}^{7} \omega_j I_{g_j}(s), \tag{1}$$

where I_{g_j} is the partial intensity corresponding to the quadrature point (or pseudo-wave number) g_j and ω_j is the associated weight. I_{g_j} is the solution of the RTE at a given point s and a given propagation direction $\vec{u}$:

$$\frac{\partial I_{g_j}(\vec{u},s)}{\partial s} = -k_{g_j} I_{g_j}(\overrightarrow{u},s) + k_{g_j}\bar{I}_v^0(s), \tag{2}$$

where $\bar{I}_v^0$ is the Planck function taken at band central wave number and k_{g_j} is the absorption coefficient at quadrature point g_j. The values of $k(g_j)$ are the CK model parameters which have been generated for applications at atmospheric pressure in the temperature range 300–2500 K [39]. These parameters have been obtained for the set of sixteen temperature values, forty four spectral intervals and a set of 5 X_{H_2O} values for H_2O, and seventeen spectral intervals for CO_2 [39].

The ADF model is a global model similar to the spectral line-based weighted-sum-of-gray-gases model due to Denison and Webb [29]. The difference appears in the calculations of weights which are chosen in such a manner that emission by an isothermal gas is rigorously predicted by the ADF model [30].

The ADF parameters are the reduced absorption coefficients $k_j^* = k_j/(Xp)$ (X being the molar fraction of the absorbing species and p the total pressure) for the gray gases j; $j = 1,\ldots,N$, and the associated weights a_j satisfying $\sum_j a_j = 1$. The parameters k_j^* and a_j were calculated at atmospheric pressure in the temperature range 300–2500 K [32]. For H_2O, these parameters were tabulated for 5 X_{H_2O} values but they do not significantly depend on X_{CO_2} when CO_2 is the absorbing gas. The chosen reference conditions were $T_{ref} = 1100$ K and X_{H_2O} or X_{CO_2} equal to 0.1. This model, called ADF8 ($N = 8$), uses seven non-zero absorption coefficients and one (equal to zero) corresponding to the transparency regions of the gas.

The total radiative intensity $I(\vec{u},s)$ is written in the ADF model as a sum of partial intensities:

$$I(\vec{u},s) = \sum_{j=1}^{N} I_j(\vec{u},s). \tag{3}$$

The partial intensity $I_j(\vec{u},s)$ satisfies the following RTE:

$$\frac{\partial I_j(\vec{u},s)}{\partial s} = k_j^*(s)X(s)p(s)\left[a_j(s)\frac{\sigma T^4(s)}{\pi} - I_j(\vec{u},s)\right]. \tag{4}$$

3. Basic formulation and methods of solution

3.1. Basic equations of fluid flow

In the present study, we consider a laminar steady flow of a non-scattering gas (H_2O or CO_2) inside a circular duct with an abrupt change of the wall temperature at the abscissa $x = l_0$ (see Fig. 1). The inlet gas temperature T_0 at the section $x = 0$ is equal to the wall temperature for $x < l_0$. For a non-radiating gas and in

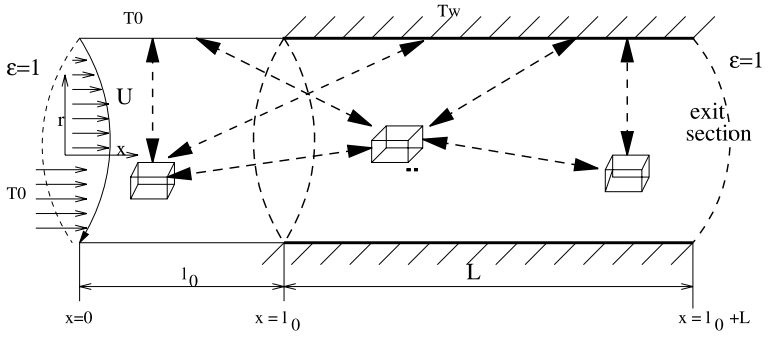

Fig. 1. Geometrical and physical conditions.

the parabolic approximation, the gas remains at T_0 until the section $x = l_0$. But for an emitting and absorbing gas, there is a preheated or precooled zone due to the action at distance of radiation. This phenomenon is taken into account in the present study.

Except for radiative transfer, the usual approximations of a boundary layer flow are made. In fact, we consider sufficiently large Peclet numbers for which the axial component of the conductive flux is negligible [40,41]. The significant temperature difference imposed between the walls and the gas requires the use of temperature-dependent fluid physical properties.

If we restrict our considerations to axially symmetric flows, the mass, momentum and energy balance equations write in cylindrical coordinates:

$$\frac{\partial(\rho r u)}{\partial x} + \frac{\partial(\rho r v)}{\partial r} = 0, \tag{5}$$

$$\frac{\partial(\rho u u)}{\partial x} + \frac{\partial(\rho u v)}{\partial r} = -\frac{\mathrm{d}p}{\mathrm{d}x} + \frac{1}{r}\frac{\partial}{\partial r}\left(r\mu\frac{\partial u}{\partial r}\right), \tag{6}$$

$$\frac{\partial(\rho u h)}{\partial x} + \frac{\partial(\rho v h)}{\partial r} = -u\frac{\mathrm{d}p}{\mathrm{d}x} + \frac{1}{r}\frac{\partial}{\partial r}\left(r\frac{\lambda}{C_p}\frac{\partial h}{\partial r}\right) + \mu\left(\frac{\partial u}{\partial r}\right)^2 - \mathrm{div}\,\vec{q}_\mathrm{r}, \tag{7}$$

where u and v are the axial and transverse velocity components, respectively. h, ρ , μ, λ and C_p designate the enthalpy per unit mass, the temperature-dependent density, viscosity, thermal conductivity and specific heat at constant pressure, respectively.

The gas (H_2O or CO_2) obeys the perfect gas law. The thermophysical properties of these gases are approximated by temperature-dependence functions generated from the data given in Ref. [42].

In the case of CK model, the divergence of the radiative flux, appearing in the energy equation, is given by:

$$\mathrm{div}\,\vec{q}_\mathrm{r} = \sum_{\text{bands } b}\Delta\nu_\mathrm{b}\sum_{j=1}^{7}\omega_j\int_{4\pi}\left[-k_{g_j,b}I_{g_j,b}(\vec{u},s) + k_{g_j,b}I^0_{\nu_\mathrm{b}}(s)\right]\mathrm{d}\Omega. \tag{8}$$

In the case of ADF model, it is given by:

$$\mathrm{div}\,\vec{q}_\mathrm{r} = \sum_{j=1}^{N=8}\int_{4\pi}k^*_j(s)X(s)p(s)\left[a_j(s)\frac{\sigma T^4(s)}{\pi} - I_j(\vec{u},s)\right]\mathrm{d}\Omega. \tag{9}$$

For both models, the same numerical procedure is used to compute $I_{g_j,\mathrm{b}}$ and I_j. This procedure is explained in the following subsection.

At the wall the no-slip condition, the impermeability of the wall, and the imposed wall temperature give the following boundary conditions:

$$u(x,R) = 0, \qquad v(x,R) = 0, \tag{10}$$

$$h(x,R) = h(T_\mathrm{w}) \text{ for } x > l_0 \quad \text{and} \quad h(x,R) = h(T_0) \text{ for } x < l_0.$$

At the centerline the following conditions arise from the symmetry of the problem:

$$\left.\frac{\partial u(x,r)}{\partial r}\right|_{r=0} = 0, \quad v(x,0) = 0 \quad \text{and} \quad \left.\frac{\partial h(x,r)}{\partial r}\right|_{r=0} = 0. \tag{11}$$

For $x = 0$ we have the starting conditions:

$$v(0,r) = 0, \quad u(0,r) = 2u_0\left(1 - \left(\frac{r}{R}\right)^2\right) \quad \text{and} \quad h(0,r) = h(T_0). \tag{12}$$

For the radiative intensity, the walls are assumed to emit and reflect isotropically with a constant emissivity ϵ_w. The hypothesis of gray walls is required in the ADF model but not in CK. It will be assumed in all this study for comparison purposes. This yields for the CK model at a wall point:

$$I_{g_j,b}(\vec{u}) = \epsilon_\mathrm{w}I^0_{\nu_\mathrm{b}}(T_\mathrm{wall}) + \frac{(1-\epsilon_\mathrm{w})}{\pi}\int_{\vec{n}\cdot\vec{u'}<0} I_{g_j,b}(\vec{u'})|\vec{n}\cdot\vec{u'}|\,\mathrm{d}\Omega, \tag{13}$$

where T_wall is equal to T_0 for $x < l_0$ and to T_w for $x > l_0$, $\vec{n}$, $\vec{u}$, $\vec{u'}$ are the direction normal to the boundary, the direction of emission and the direction of incoming radiation respectively. For the ADF model, the radiative boundary condition writes:

$$I_j(\vec{u}) = \epsilon_\mathrm{w}a_j(T_\mathrm{wall})\frac{\sigma T^4_\mathrm{wall}}{\pi} + \frac{(1-\epsilon_\mathrm{w})}{\pi}\int_{\vec{n}\cdot\vec{u'}<0} I_j(\vec{u'})|\vec{n}\cdot\vec{u'}|\,\mathrm{d}\Omega. \tag{14}$$

In addition, the inlet section ($x = 0$) is considered for radiative transfer as a black wall at temperature T_0 while the outlet section ($x = l_0 + L$) is a black wall at T_w. L is chosen sufficiently large so that this last condition has no incidence on the results near $x = l_0$.

3.2. Solution of the radiative transfer equation

The main advantage of CK and ADF approaches, as compared to SNB models used in Refs. [34–36], is that the radiative properties are described in terms of absorption coefficients. The RTE retains thus the same mathematical form as the spectral equation and will be compatible with any RTE solver and can be applied without further approximations to reflecting walls.

We use in this study the discrete-direction method, developed initially for radiative transfer in axisymmetric systems using statistical narrow-band models. This method is adapted here to CK and ADF models which

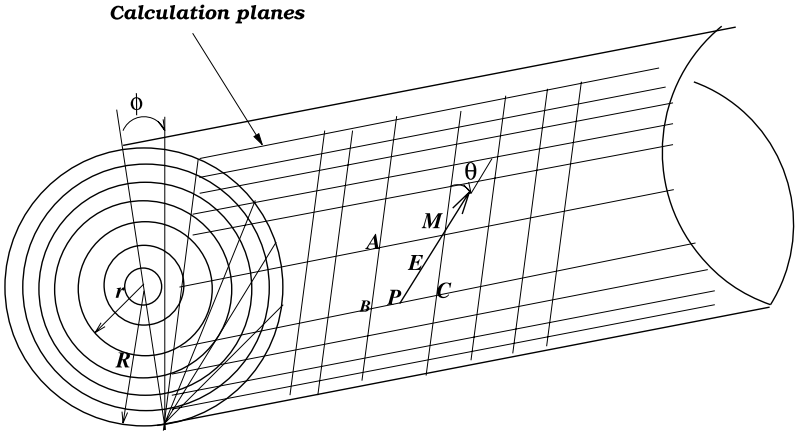

Fig. 2. Spatial and directional discretizations for radiative transfer.

do not require the recourse to approximations such as the ellipsoid correlation coefficient [34]. The discrete-direction method is close to the discrete ordinates method except for (i) the directional integration quadrature: a regular integration with prescribed angular increments and solid angles is used here, (ii) intensity interpolations are used instead of integrations over control volumes. We take advantage of the system axisymmetry by only doing calculations in the planes shown schematically in Fig. 2.

We give in this section the modifications introduced by the use of these models. A detailed description of this method applied with the SNB or with the WSGG models are given in Refs. [34–36]. In order to compute the radiative flux and radiative powers, the method uses two discretizations: (i) a spatial discretization which consists in defining the radial and axial grid points where radiative intensities are calculated, (ii) a directional discretization of the two angles ϕ and θ as shown in Fig. 2. The discretization of ϕ is based on the radial discretization. The calculations are carried out in the planes parallel to the system axis and tangential to the coaxial cylinders, defined by the radial discretization.

For each plane and each transfer direction θ, the radiative intensity at a point M is step by step calculated by using interpolations between upstream grid points where the intensities are known.

For the CK model and for a direction θ as shown for instance in Fig. 2, the intensity at M is given by:

$$I_{g_j,\mathrm{b}}(\vec{u},M) = I_{g_j,\mathrm{b}}(\vec{u},P)\exp(-k_{g_j,\mathrm{b}}(E)l) + [1-\exp(-k_{g_j,\mathrm{b}}(E)l)]I^0_{\nu_\mathrm{b}}(T(E)). \quad (15)$$

This expression is replaced for the ADF model by:

$$I_j(\vec{u},M) = I_j(\vec{u},P)\exp(-k^*_j(E)Xpl) + [1-\exp(-k^*_j(E)Xpl)]a_j(E)\frac{\sigma T_E^4}{\pi}. \quad (16)$$

In both cases, the intensity at point M is obtained from linear interpolation of the known intensities at the neighbor grid points. The use of the above equations and the radiative boundary condition for each direction inside each plane leads to a system of linear equations where the unknowns are the intensities leaving the wall points. After the inversion of this system, the intensities inside the volume are computed from Eq. (15) or (16). The volumetric radiative power is then calculated directly from the intensity field and Eq. (8) or (9).

3.3. Numerical solution procedure

The system of equations described in Section 3.1 is inherently elliptic if 2-D radiation calculations are used. The ellipticity is caused by the radiative term which is characterized by its action at distance. The marching solution procedure in the axial direction cannot be applied without the knowledge of the radiative dissipation field at each point of the system. We propose in this study a numerical method able to transform the elliptic problem to a series of parabolic ones where the marching solution can be used.

The proposed method starts first with the prediction of the temperature and velocity fields using local 1-D radiative transfer calculations and a marching procedure along the axial direction. The radiative source term for a given section i is calculated from a one-dimensional temperature field assuming $T(x,r) = T(x_{i-1},r)$, where x_{i-1} designates the previous section. In practice, the same numerical procedure explained above for radiative transfer calculations is used with six discretized axial sections and a very large spacing between these sections in comparison with the tube diameter. The results of this first step will be called 1-D radiation results in the following.

In a second step, an iterative procedure is undertaken. Two-dimensional radiative powers and fluxes are

calculated from the 2-D temperature field and then the flow and energy equations are solved using the marching procedure and the computed radiative powers as source terms. Global iterations between these sequences are performed until convergence of the temperature and radiation fields. This iterative procedure starts with the 1-D radiation temperature field for the 2-D calculation of the radiative field. The required number of global iterations depends on the optical thickness of the medium. For a tube diameter D equal to 2 cm, only two iterations are required while for $D = 20$ cm, an underrelaxation of the radiative powers is required for convergence and four to five global iterations are required.

For the computation of velocity and temperature fields, a marching implicit finite volume procedure based on the pressure correction algorithm [43] is used. Mass, momentum and energy equations are solved simultaneously in order to account for variable fluid properties. This procedure has been validated by comparison with the results of Ref. [44] in the case of variable fluid properties but without radiative transfer.

A constant mesh size is used for the radial direction and a variable one in the axial direction. This mesh size increases far from the entrance, which allows a higher accuracy for the temperature and velocity fields in the thermal entrance region where steep axial gradients occur. Typically, we use 80 radial points for $D = 20$ cm and 8000 axial ones to compute the flow field along ten tube diameters. A such refined grid is not required for 2-D radiation calculations; numerical tests show that typically 20×100 nodes are sufficient for the above configuration with a H_2O flow. Numerical interpolations and extrapolations are used to convert the results from the convective grid mesh to the radiative one and vice versa.

4. Results and discussion

Calculations have been carried out for $D = 2$ and 20 cm, for pure H_2O or pure CO_2 at atmospheric pressure as radiating gases, and for heated ($T_0 = 500$ K, $T_w = 1500$ K) and cooled ($T_0 = 1500$ K, $T_w = 500$ K) fluid. The velocity inlet profile is parabolic in all cases. The 2 cm diameter corresponds to a relatively optically thin medium (especially for H_2O). The same calculations have been done for the same gases considered as transparent. It was found to be sufficient to take an upstream region length l_0 equal to $5D$ for $D = 2$ cm and equal to D for $D = 20$ cm. Echigo et al. [2], limited by numerical constraints, have chosen $l_0 = 0.45D$ and $L = 1.05D$ for convection, and the radiation contribution is considered in the region from $-1.5D$ to $1.5D$ around an arbitrary section x. Baek et al. [7] have selected the same domain for both convection and radiation with $l_0 = 1.95D$ and $L = 2.55D$.

The Reynolds numbers were chosen sufficiently large ($\geqslant 500$) in order to neglect the effects of axial conduction. When not specified, the Reynolds number (with fluid properties taken at T_0) is equal to 2000. The walls are assumed black in all the calculations presented here. Although calculations have been carried out with various emissivities, we limit ourselves to black walls in this presentation for the sake of clarity. The presentation and discussion of the results will be divided in two subsections. Coupled heat transfer characteristics and detailed comparisons between 1-D and 2-D radiation are given in Section 4.1. These results are obtained from the CK model. A detailed comparison between results from ADF and CK models is then provided in Section 4.2. Due to the non-linearities, in particular in the energy equation, and to the complexity of molecular spectra, the results are presented in terms of dimensional quantities.

The effects of radiative transfer on the velocity field, in particular through the temperature field and the variable fluid properties, are not discussed here.

We use the following convention: the radiative wall flux is the difference between the absorbed and the emitted flux, and the radiative power will designate the volumetric power emitted by the medium minus the absorbed power, i.e., $\mathrm{div}\,\vec{q}_r$.

4.1. Coupled transfer characteristics and 2-D versus 1-D radiation calculations

The wall radiative fluxes for cooling and heating H_2O in the upstream ($x < l_0$) and in the downstream ($x > l_0$) regions are shown in Fig. 3a and b for $D = 2$ and 20 cm, respectively. The results from both one-dimensional and two-dimensional radiation analyses are presented. The 1-D wall flux in the upstream region ($x < l_0$) is equal to zero and is not shown. The 1-D radiative wall flux in the downstream region is always smaller (in absolute value) than the 2-D one since it does not take into account wall to wall radiative transfer. The difference between these fluxes decreases far from the thermal entrance section since the radiative wall flux becomes mostly due to gas to wall transfer. For the thin case ($D = 2$ cm), the absolute wall radiative flux is greater when the gas is heated than when it is cooled. However, for the thick case ($D = 20$ cm), an opposite result is obtained. In fact, although hot bands appear in H_2O spectra at high temperature, its total emissivity is higher at 500 K than at 1500 K. But for $D = 20$ cm, as will be seen later, the difference between the gas bulk temperature and the wall temperature is much more rapidly reduced for a heated gas than for a cooled gas at constant inlet Reynolds number. This explains the higher absolute radiative wall flux when the gas is cooled for $D = 20$ cm.

Typical results of radial temperature and radiative power profiles at different sections are plotted in Figs. 4–6.

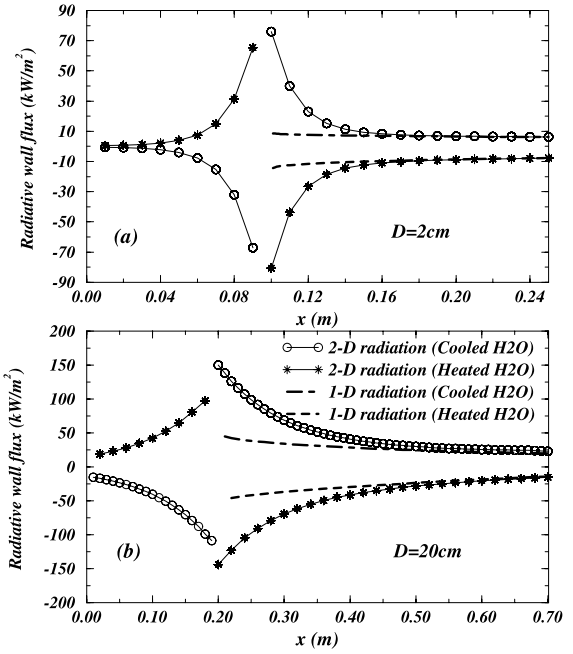

Fig. 3. 1-D and 2-D radiative wall fluxes for heated and cooled H_2O: (a) $D = 2$ cm and (b) $D = 20$ cm.

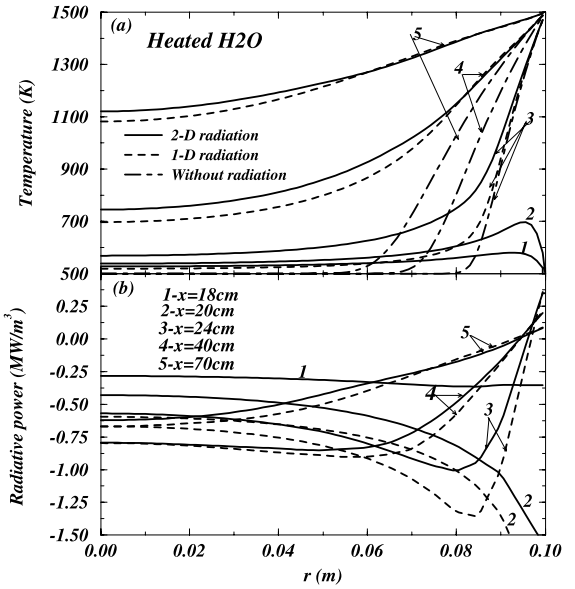

Fig. 4. Effects of axial radiation on heated H_2O flow. Radial distribution of temperature (a) and of radiative power (b) at different sections: $D = 20$ cm, $Re = 2000$, $T_0 = 500$ K and $T_w = 1500$ K.

Results from calculations using 1-D and 2-D radiation, as well as results without radiation are presented. Figs. 4–6 correspond to heated H_2O, heated CO_2 and cooled H_2O, respectively, with $D = 20$ cm in all cases. Lines 1 and 2 in these figures correspond to $x = 18$ cm and $x = l_0 = 20$ cm, respectively. The corresponding temperature profiles are not shown for calculations without radiation or with 1-D radiation since gas temperature is still uniform and equal to T_0. Line 2 for 1-D radiative power corresponds to calculations carried out just after $x = l_0$ ($x = l_0 + 1 \times 10^{-5}$ m).

It is shown on Fig. 4a that the fluid is preheated before the section $x = l_0$ when 2-D radiation is considered. This classical result, due to the propagation of thermal radiation into the region upstream is pointed out in Refs. [2,5,7]. Due to the relatively high-optical thickness in this case, the preheating is more important close to the walls than in the center region. A difference between the temperatures computed by using 1-D and 2-D radiation takes place and remains noticeable as long as the difference between wall and bulk fluid temperatures is significant. Although the 1-D radiation overestimates the radiative power as seen in Fig. 4b, the computed bulk temperature is smaller than that obtained with 2-D radiation calculations. Such phenomenon can be explained by the existence of the preheated region. The absolute value of the 2-D radiative power is smaller than the corresponding 1-D one since, on one hand, the 2-D radiation bulk temperature is higher than

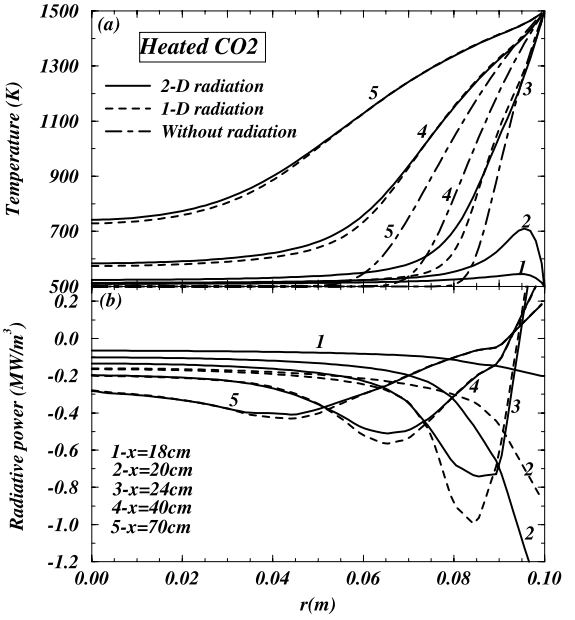

Fig. 5. Effects of axial radiation on heated CO_2 flow. Radial distribution of temperature (a) and of radiative power (b) at different sections: $D = 20$ cm, $Re = 2000$, $T_0 = 500$ K and $T_w = 1500$ K.

the 1-D one and, on the other hand, the axial part of the radiative flux induces significant energy transfer from

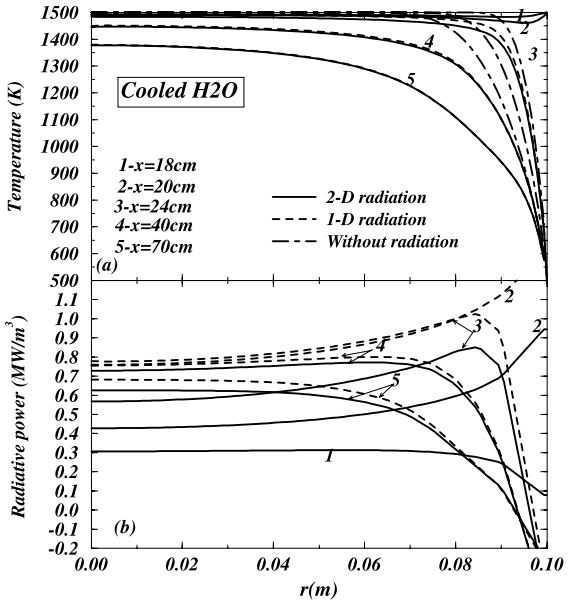

Fig. 6. Effects of axial radiation on cooled H_2O flow. Radial distribution of temperature (a) and of radiative power (b) at different sections: $D = 20$ cm, $Re = 2000$, $T_0 = 1500$ K and $T_w = 500$ K.

downstream to upstream regions. For heated CO_2, the evolution of temperature and radiative power profiles are plotted in Fig. 5a and b, respectively. The effects of 2-D radiation are similar to those discussed for H_2O. One difference with H_2O results is that the maximum of the absolute radiative power is more pronounced. This is due to the structure of CO_2 spectrum which is characterized by strong vibrational bands near 4.3 μm. These bands become optically thick and prevent efficient transfer to the center of the duct. In fact, as pointed out by Echigo et al. [2], in the case of a large optical thickness, the radiation energy cannot travel into the deep central core even if the wall is kept at high temperature and emits radiation intensively. Such radiative behavior modifies also the temperature profile shapes by introducing pronounced inflexion points in the case of CO_2. The evolution of temperature profiles given in Figs. 4a and 5a shows that the wall to gas radiative transfer is globally less efficient for CO_2 than for H_2O. In spite of a smaller value of $\dot{m}C_p$, where $\dot{m}$ is the mass flow rate, the temperature level for CO_2 is lower than the one observed for H_2O.

For cooled H_2O, it is shown on Fig. 6 that the radiative power is of the same magnitude than when the same gas is heated. In fact, its total emissivity is smaller at high temperature but the difference between wall temperature and the fluid bulk temperature is much greater for cooled H_2O. This is a simple consequence of a higher mass flow rate due to viscosity variations with temperature and the use of a constant Reynolds number. The 1-D radiation calculations overestimates here also the absolute radiative power; but in this case, this is only due to the axial radiative transfer from the upstream regions to a given section. Another difference with the heating case is that, in spite of the existence of the precooling region, the difference between 1-D and 2-D radiation temperature vanishes after about three diameters in the case of cooled H_2O.

Fig. 7 shows the evolution of the bulk temperatures computed with 1-D and 2-D radiation for heated H_2O or CO_2 flows and for different values of the Reynolds number with $D = 20$ cm. As discussed for $Re = 2000$, the difference between 1-D and 2-D radiation calculations remains noticeable as long as the difference between wall and bulk fluid temperatures is significant. This result was observed for all Reynolds numbers and heated gases. For $Re = 500$, the preheating of H_2O by radiation is very important and leads to a bulk temperature increase of about 300 K at the section $x = l_0$.

The calculations without radiation presented in Figs. 4a, 5a, 6a and 7 show that, for the conditions of these figures, radiative transfer is much more efficient than the conductive one.

Fig. 8a and b shows the evolution of the heat transfer coefficients in the downstream region for heated and cooled H_2O, respectively, with $D = 20$ cm. These total, conductive and radiative transfer coefficients are defined as:

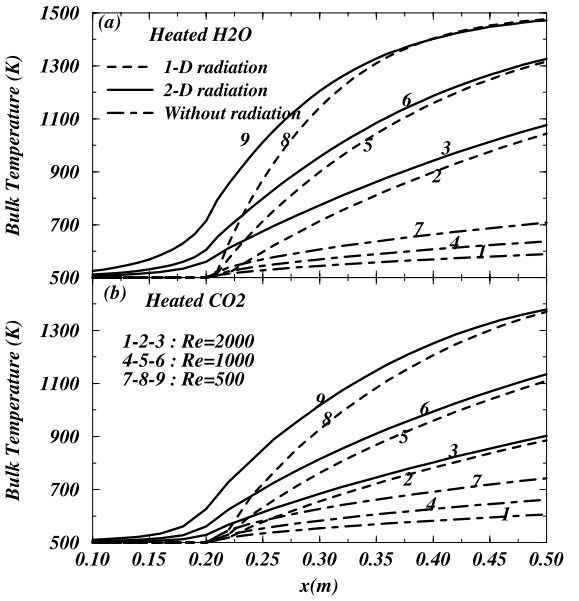

Fig. 7. Effects of the Reynolds number on the evolution of bulk temperature: $D = 20$ cm, $T_0 = 500$ K and $T_w = 1500$ K. (a) Heated H_2O and (b) heated CO_2.

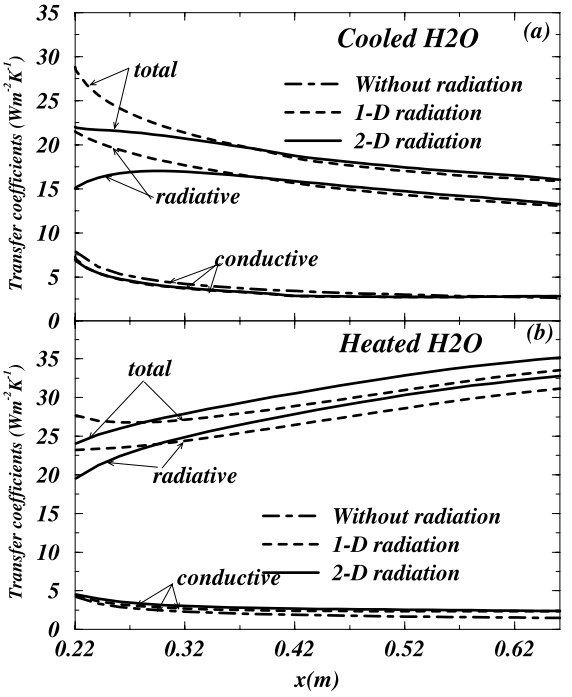

Fig. 8. Effect of axial radiation on the local heat transfer coefficients ($D = 20$ cm, $Re = 2000$). (a) Cooled H_2O ($T_0 = 1500$ K, $T_w = 500$ K) and (b) heated H_2O ($T_0 = 500$ K, $T_w = 1500$ K).

$$H_{tt}(x) = \left| \frac{\varphi_{tt}(x)}{T_w - T_b(x)} \right|, \quad H_{cd}(x) = \left| \frac{\varphi_{cd}(x)}{T_w - T_b(x)} \right|,$$
$$H_r(x) = \left| \frac{\varphi_r(x)}{T_w - T_b(x)} \right|,$$

where the conductive, radiative and total fluxes are given by:

$$\varphi_{cd}(x) = -\lambda \left. \frac{\partial T(x,r)}{\partial r} \right|_{r=R},$$
$$\varphi_r(x) = \frac{\int_S \operatorname{div} \vec{q}_r \, dS}{2\pi R}, \quad \varphi_{tt}(x) = \varphi_{cd}(x) + \varphi_r(x).$$

The radiative flux $\varphi_r(x)$ corresponds to the radiative power integrated over a cross-sectional area S. Thus, $2\pi R \varphi_r(x)\,dx$ represents the amount of radiative energy exchanged between the cylindrical element of width dx and all its surroundings (wall and other gas elements). This flux should be used when writing the evolution equation of the bulk temperature. Contrary to the wall radiative flux, it does not take into account wall-to-wall radiative transfer in the case of 2-D radiation calculations.

Fig. 8a and b show that the total transfer coefficients computed with radiation are of course higher than the ones obtained without radiation. The conductive transfer coefficient H_{cd} increases when considering radiation in the case of heated H_2O and decreases for cooled H_2O. For the 1-D radiation calculations, the evolution of the transfer coefficients is similar to that described in Ref. [19] for H_2O flowing inside a plane channel. The radiative transfer coefficient H_r computed with 2-D radiation is greater than that obtained by the 1-D radiation calculation beyond 1.5 diameter distance from the section $x = l_0$, though the 1-D radiative power is greater than that obtained by the 2-D one (see Fig. 4). This result is explained by the fact that the absolute difference $|T_w - T_b|$ is lower when 2-D radiation is taken into account. An opposite result is obtained in the downstream region close to $x = l_0$; gas-to-gas exchange with the preheated (or the precooled) zone leads to a smaller radiative transfer coefficient in this region when the axial radiative transfer is accounted for.

4.2. Comparison between results from ADF and CK models

Fig. 9a and b show the radial evolution of the volumetric radiative power at different sections for heated and cooled H_2O, respectively, computed from CK and ADF models with $D = 20$ cm. The radiative power is slightly overestimated by the ADF model for a gas hotter than the wall but it is underestimated (in absolute value) for a heated gas. The difference between the two

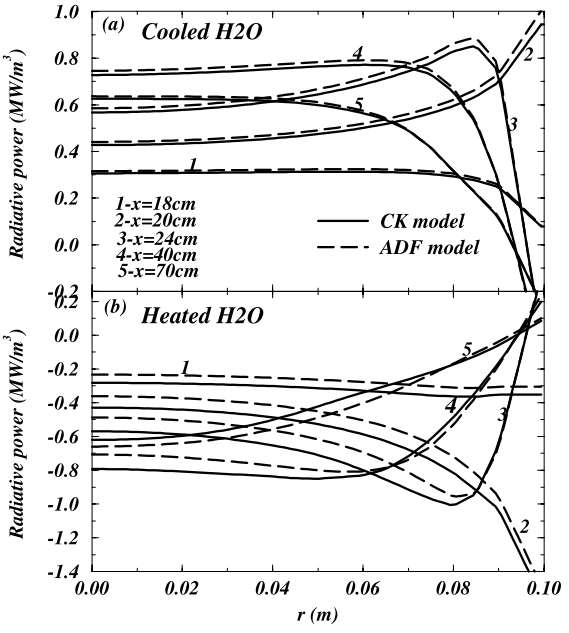

Fig. 9. Comparison between CK and ADF model results. Radial distribution of radiative power for cooled H_2O ($T_0 = 1500$ K and $T_w = 500$ K) (a) and for heated H_2O ($T_0 = 500$ K and $T_w = 1500$ K) (b) at different sections: $D = 20$ cm, $Re = 2000$.

models is larger when gaseous absorption is the dominant phenomenon. This is due to the less accurate prediction of absorption by the ADF model. This result is in agreement with the results of Ref. [31] where the underestimation of absorption by a cold gas in the ADF model is analyzed in terms of the correlation assumption used in this model. Let us recall that the correlation assumption in the ADF model has been built to yield accurate predictions of the total emissivity of uniform columns.

Fig. 10 presents the evolution of bulk temperatures for heated and cooled H_2O calculated by using CK and ADF with a diameter equal to 20 or 2 cm. The prediction of bulk temperature when using ADF model is as expected significantly better for cooled H_2O than for heated H_2O. For an optically thin ($D = 2$ cm) heated gas, although the relative difference between the radiative fluxes from both models is the same as for 20 cm, the effect on bulk temperature is smaller. This is due to the predominance of the conduction mode in this case (for $D = 2$ cm, $\varphi_{cd} \approx 2\varphi_r$).

For heated H_2O, it is worth noticing that the differences observed for radiative powers calculated from both models are not due to the bulk temperature variation. In fact, although the difference $|T_b - T_w|$ computed by using CK model is smaller than that computed by using ADF model, the result of radiative power calculations are opposite ($|P_R^{CK}| > |P_R^{ADF}|$). Thus, there is a balance effect which leads to errors on the bulk temperature smaller than the ones on the radiative fluxes.

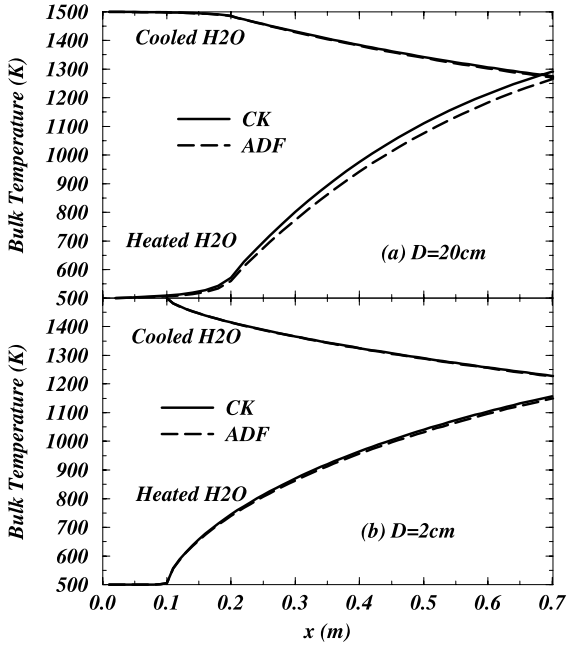

Fig. 10. Comparisons between CK and ADF model results. Evolution of bulk temperature for heated ($T_0 = 500$ K and $T_w = 1500$ K) and cooled ($T_0 = 1500$ K and $T_w = 500$ K) H_2O: (a) $D = 20$ cm and (b) $D = 2$ cm.

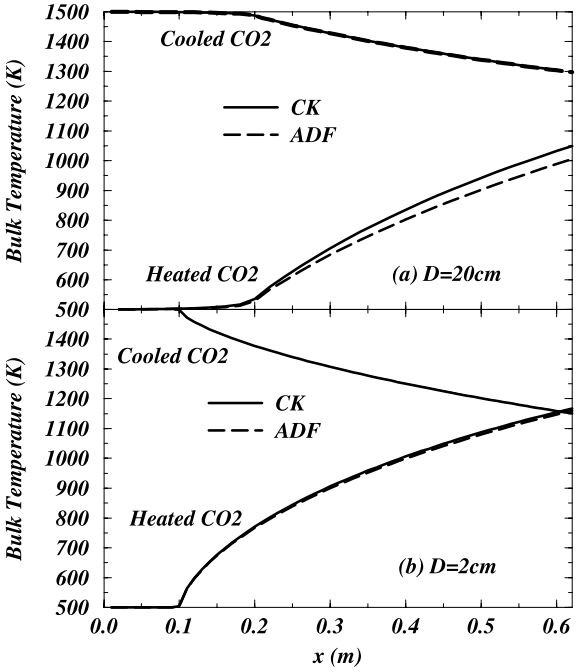

Fig. 11. Comparisons between CK and ADF model results. Evolution of bulk temperature for heated ($T_0 = 500$ K and $T_w = 1500$ K) and cooled ($T_0 = 1500$ K and $T_w = 500$ K) CO_2: (a) $D = 20$ cm and (b) $D = 2$ cm.

Fig. 11 shows the evolution of bulk temperatures computed by using the ADF and CK models for D equal to 20 cm or to 2 cm in the case of heated and cooled CO_2. The previous tendencies are observed again, but for a diameter equal to 20 cm, the difference between model results is more pronounced when CO_2 is heated. The relative error, $|T_b^{CK} - T_b^{ADF}|/|T_b^{CK} - T_0|$, induced by ADF reaches 12%.

We turn now to the comparison of the CPU times required by both models.

As pointed out in Refs. [31,32], the computing times for absorption coefficient based models depend on the number of discretized pseudo-spectral locations for which the RTE is solved (for fixed spatial and directional discretizations).

Concerning the CK model, the CPU required time in the case of CO_2 is smaller than that corresponding to H_2O due to the transparency regions of CO_2. The ratio between the two CPU times is about 2.5 for one radiation calculation.

The ratio between CK and ADF CPU times required for a 2-D radiation calculation coupled to convection for H_2O is about 30. This ratio is close to the one found in Refs. [31,32] for pure radiation calculations. The CPU

times required for the flow calculations in the applications considered here are very small.

For applications involving H_2O–CO_2 mixtures with non-uniform ratio of molar fractions, the ADF CPU time increases less rapidly since the overlapping between H_2O and CO_2 spectra occurs only for a few narrow bands [30].

5. Conclusion

The coupled radiation-laminar forced convection problem in the entrance region of a duct was studied numerically for strongly non-isothermal real gases. The test problem consisted of a flowing gas (H_2O or CO_2) inside a tube with a sudden jump of wall temperature. The axial component of the radiative flux was taken into account and its effects on the evolution of temperature profiles was analyzed. A detailed comparison between the results from a band model (CK) and a global model (ADF), employed to represent the molecular radiative properties, is provided. The main conclusions of this study can be summarized as follows:

- The length of the preheated or precooled zone for H_2O and CO_2 flows is typically one half diameter upstream the section corresponding to the change of wall temperature. The spectral nature of gas radiative properties led to different temperature and radiative power profiles for H_2O and CO_2, with a radiation blocking effect in the case of CO_2 due to the intense bands near 4.3 μm. Such effects cannot be predicted by using a gray gas approach.
- Contrary to the conclusions of some authors, we found that the effects of the radiative axial component remain noticeable as long as the difference between wall and fluid bulk temperatures is significant. This is mainly due to the preheating or precooling effect which is very important for low-Reynolds numbers and relatively thick media. As a result of the same effect, we found that although the 1-D radiation analysis overestimates the radiative power, the absolute difference between wall and bulk temperatures is smaller when 2-D radiation is considered.
- Comparisons between ADF and CK results showed that ADF results are less accurate when the gas is heated than when it is cooled. Only small discrepancies are observed in temperature and radiative fields when H_2O or CO_2 is cooled while, as a result of a less accurate prediction of absorption by the ADF model, differences up to 12% on the bulk temperatures (scaled by $|T_b - T_0|$) are observed for the studied heated gases. Although the ADF model consumes less computer times, it remains limited to gray walls and, in more general applications, also to gray participating particles.

References

[1] S. Desoto, Coupled radiation conduction and convection in entrance region flow, Int. J. Heat Mass Transfer 11 (1968) 39–53.
[2] R. Echigo, S. Hasegawa, K. Kamiuto, Composite heat transfer in a pipe with thermal radiation of two dimensional propagation in convection with the temperature rise in flowing medium upstream from heating section, Int. J. Heat Mass Transfer 18 (1975) 1149–1159.
[3] M. Kassemi, B.T.F. Chung, Two-dimensional convection and radiation with scattering from a Poiseuille flow, J. Thermophys. Heat Transfer 4 (1) (1990) 98–105.
[4] T.K. Kim, H.S. Lee, Two-dimensional anisotropic scattering radiation in thermally developing Poiseuille flow, J. Thermophys. Heat Transfer 4 (3) (1990) 292–298.
[5] J.H. Huang, J.D. Lin, Radiation and convection in circular pipe with uniform wall heat flux, J. Thermophys. Heat Transfer 5 (4) (1991) 502–507.
[6] G. Yang, M.A. Edabian, Thermal radiation and laminar forced convection in the entrance region of a pipe with axial conduction and radiation, Int. J. Heat Fluid Flow 12 (3) (1991) 202–209.
[7] S.W. Baek, J.M. Yu, T.K. Kim, Thermally developing Poiseuille flow affected by radiation, Numer. Heat Transfer, Part A 35 (1999) 681–694.
[8] B.E. Pearce, A.F. Emery, Heat transfer by thermal radiation and laminar forced convection to an absorbing fluid in the entry region of a pipe, J. Heat Transfer 92 (1970) 221–230.
[9] K.H. Im, R.K. Ahluwalia, Combined convection and radiation in rectangular ducts, Int. J. Heat Transfer 27 (2) (1984) 221–231.
[10] A.T. Wassel, D.K. Edwards, Molecular gas radiation in a laminar or turbulent pipe flow, J. Heat Transfer 98 (1976) 101–107.
[11] A. Balakrishnan, D.K. Edwards, Molecular gas radiation in the thermal entrance region of a duct, J. Heat Transfer 101 (1979) 489–495.
[12] T. Seo, D.A. Kaminski, M.K. Jensen, Combined convection and radiation in simultaneously developing flow and heat tran sfer with nongray gas mixtures, Numer. Heat Transfer, Part A 26 (1994) 49–66.
[13] K. Kamiuto, Combined laminar forced convection and non-gray radiation heat transfer to carbon dioxide flowing in a non black plane-parallel duct, Numer. Heat Transfer, Part A 28 (1995) 575–587.
[14] T.K. Kim, R. Viskanta, Interaction of convection and radiation heat transfer in high pressure and temperature steam, Int. J. Heat Mass Transfer 27 (6) (1984) 939–941.
[15] T.F. Smith, Z.F. Shen, A.M. Alturki, Radiative and convective transfer in a cylindrical enclosure for a real gas, J. Heat Transfer 107 (1985) 482–485.
[16] T.F. Smith, C.W. Clausen, Radiative and convective transfer for tube flow of a real gas, Int. Heat Transfer Conf. 3 (1978) 391–396.
[17] N.K. Nakra, T.F. Smith, Combined radiation-convection for a real gas, J. Heat Transfer 99 (1977) 60–65.
[18] C.W. Clausen, T.F. Smith, Radiative and convective transfer for a real gas flow through a tube with specified wall heat flux, J. Heat Transfer 101 (1979) 376–378.

[19] A. Soufiani, J. Taine, Application of statistical narrow-band model to coupled radiation and convection at high temperature, Int. J. Heat Mass Transfer 30 (1987) 437–447.
[20] C. Mesyngier, B. Farouk, Convection non-gray gas radiation interactions in a channel flow, ASME Natl. Heat Transfer Conf., HTD 325 (1996) 103–113.
[21] S. Tabanfar, M.F. Modest, Combined radiation and convection in absorbing, emitting, nongray gas-particulate tube flow, J. Heat Transfer 109 (1987) 478–484.
[22] M.F. Modest, Radiative Heat Transfer, McGraw-Hill, New York, 1993.
[23] R. Viskanta, Overview of convection and radiation in high temperature gas flows, Int. J. Engng. Sci. 36 (1998) 1677–1699.
[24] W. Malkmus, Random Lorentz band model with exponential-tailed S^{-1} line-intensity distribution, J. Opt. Soc. Am. 57 (1967) 323–329.
[25] R.M. Goody, Y.L. Yung, Atmospheric Radiation: Theorical Basis, Oxford University Press, Oxford, 1989.
[26] Ph. Rivière, A. Soufiani, J. Taine, Correlated-k and fictitious gas methods for H_2O near 2.7 μm, J. Quant. Spectrosc. Radiat. Transfer 48 (1992) 187–203.
[27] R. Levi di Leon, J. Taine, Fictive-gas-method for accurate computations of low-resolution IR gas transmissivities: application to the 4.3 μm CO_2 band, Revue de Physique Appliquée 21 (1986) 825–831.
[28] D.K. Edwards, Molecular gas band radiation, in: J.P. Hartnett, T.F. Irvine (Eds.), Advances in Heat Transfer, vol. 12, Academic Press, New York, 1976, pp. 115–193.
[29] M.K. Denison, B. Webb, The spectral-line-based weighted-sum-of-gray-gases model in nonisothermal nonhomogeneous media, J. Heat Transfer 117 (1995) 359–365.
[30] J. Taine, A. Soufiani, Gas IR radiatives properties: from spectroscopic data to appoximate models, in: J.P. Hartnett, T.F. Irvine (Eds.), Advances in Heat Transfer, vol. 33, Academic Press, New York, 1999, pp. 295–414.
[31] L. Pierrot, A. Soufiani, J. Taine, Accuracy of narrow band and global models for radiative transfer in H_2O, CO_2 and H_2O–CO_2 mixtures at high temperature, J. Quant. Spectrosc. Radiat. Transfer 62 (1999) 523–548.
[32] L. Pierrot, Développement étude critique et validation de modèles de propriétés radiatives infrarouges de CO_2 et H_2O à haute température, Application au calcul des tranferts dans des chambres aéronautiques et à la télédètection, Thèse de Doctorat Ecole Centrale, Paris, 1997.
[33] H.C. Hottel, Sarofim. Radiative Transfer, McGraw-Hill, New York, 1967.
[34] L. Zhang, A. Soufiani, J. Taine, Spectral correlated and non correlated radiative transfer in a finite axisymmetric system containing an absorbing and emitting real gas-particle mixture, Int. J. Heat Mass Transfer 31 (1988) 2261–2272.
[35] A. Soufiani, E. Djavdan, A comparison between weighted sum of gray gases and statistical narrow-band radiation models for combustion applications, Combust. Flame 97 (1994) 240–250.
[36] A. Soufiani, J. Taine, Spectrally correlated radiative transfer in real 3D axisymmetrical systems (The Sc. Art code) The sixth International Symposium on Transport Phenomena in Thermal Engineering, Begell House Inc. Publishers, 1993, pp. 185–190.
[37] Ph. Rivière, S. Langlois, A. Soufiani, J. Taine, An approximate data base of H_2O infrared lines for high temperature applications at low resolution. Statistical narrow-band models parameters, J. Quant. Spectrosc. Radiat. Transfer 53 (1995) 221–234.
[38] D. Scutaru, L. Rosenman, J. Taine, Approximate band intensities of CO_2 hot bands at 2.7, 4.3 and 12 μm for high temperature and medium resolution applications, J. Quant. Spectrosc. Radiat. Transfer 52 (1994) 765–781.
[39] Ph. Rivière, D. Scutaru, A. Soufiani, J. Taine, A new ck data basis suitable from 300 to 2500 K for spectrally correlated radiative transfer in CO_2–H_2O transparent gas mixtures, in: G. Hewitt (Ed.), Proceedings of the 10th Heat Transfer Conference, vol. 2, Brighton, 1994, pp. 129–134.
[40] R. Singh, Heat transfer by laminar flow in a cylindrical tube, Appl. Sci. Res. (section A) 10 (1958) 325–340.
[41] P.J. Schneider, Effect of axial fluid conduction on heat transfer in the entrance regions of parallel plates and tubes, Trans. Amer. Soc. Mech. Engs. 79 (1957) 765–773.
[42] Y.S. Touloukian, P.E. Liley, S.C. Saxena, in: Thermophysical Properties of Matter, vol. 3, IFI/Plenum, New York/Washington, 1970;
Y.S. Touloukian, S.C. Saxena, P. Hestermans, in: Thermophysical Properties of Matter, vol. 11, IFI/Plenum, New York/Washington, 1970.
[43] S.V. Patankar, D.B. Spalding, A calculation procedure for heat, mass and momentum transfer in three-dimensional parabolic flows, Int. J. Heat Mass Transfer 15 (1972) 1787–1806.
[44] C.A. Bankston, D.M. McEligot, Turbulent and laminar heat transfer to gases with varying properties in the entry region of circular ducts, Int. J. Heat Mass Transfer 13 (1970) 319–343.